2016

The Effectiveness of using Total System Power for Fault Detection in Rooftop Units

Andrew L. Hjortland
Purdue University - Herrick Laboratory, United States of America, ahjortla@purdue.edu

James E. Braun
Purdue University - Herrick Laboratory, United States of America, jbraun@purdue.edu

Mikhail Gorbounov
United Technologies Research Center, East Hartford, CT, United States of America, gorboumb@utrc.utc.com

The Effectiveness of using Total System Power for Fault Detection in Rooftop Units

Andrew L. HJORTLAND[1]*, James E. BRAUN[1], Mikhail GORBOUNOV[2]

[1]Purdue University
Ray W. Herrick Laboratories
West Lafayette, Indiana, USA
{ahjortla,jbraun}@purdue.edu

[2]United Technologies Research Center
East Hartford, Connecticut, USA

* Corresponding Author

ABSTRACT

Previous research has been presented that suggests using instantaneous system power measurements to perform fault detection for rooftop units. The methodology involves generating a normal system power model using measurements of system power and outdoor-air temperature, which are then used to determine if system performance has deviated due to the presence of faults. In order to evaluate the viability of this approach, the current work presents data collected from several rooftop units subjected to different faults and ambient conditions using psychrometric chamber test facilities. The results of the testing show that total system power is not very sensitive to many common faults affecting direct-expansion air-conditioning equipment. As a further evaluation step, the fault detection methodology is applied to 5 RTUs serving a restaurant. The results of this indicate that due to the expected uncertainty in the modeled power consumption of each unit, fault detection thresholds may not be sensitive enough to detect common faults. Ultimately, the sensitivity of steady state power consumption to most faults is not sufficient given the measurement uncertainty observed and may lead to unreliable fault detection performance.

1. INTRODUCTION

A significant hurdle to widespread adoption of automated fault detection and diagnostics (AFDD) technologies for heating, ventilation, and air-conditioning (HVAC) equipment is the additional instrumentation costs associated with the required sensors and communications interfaces not traditionally installed on equipment. Packaged rooftop air conditioners (RTUs) are especially sensitive to these instrumentation cost barriers since these systems are often manufactured without or with very few sensors useful for monitoring equipment performance. Moreover, the competitive landscape and market forces have made business cases surrounding technologies that do not lead to direct improvements in equipment ratings challenging.

In order to reduce instrumentation costs, fault detection (FD) approaches have been proposed that monitor a specific performance indicator over time to determine whether faulty operation has occurred. For instance, a virtual cooling capacity sensor approach using refrigerant-side temperature measurements has been developed and applied to RTUs to detect when degradation in capacity has occurred (Li and Braun 2007; Kim and Braun 2016; Wang et al. 2016). Alternatively, electrical power measurements have been proposed for detecting common faults in RTUs (Armstrong et al. 2006; Taasevigen et al. 2015). In essence, these methodologies monitor an indicator of equipment performance and compare the current measurement with some model estimate based on normal or expected operation. While this precludes diagnosis of faults in some previously described methodologies, detection of faults when significant impacts occur is possible.

In this work, a comparison of the impacts of common faults on steady-state system electrical power is presented. The results presented are derived from data collected from several RTUs in psychrometric chamber test facilities. The configurations of the RTUs as well as the methodologies to impose and measure the severity of different faults are described in Section 2. The experimentally measured fault impacts for improper refrigerant charge level, condenser fouling, and evaporator fouling faults are also presented in Section 2.

In Section 3, the results of continuously monitoring the electrical power consumption of several RTUs installed at a restaurant are described and presented. In this section, a fault detection methodology originally proposed by Taasevigen et al. (2015) that only requires measurements of system power and outdoor air temperature are applied to the data collected from the RTUs installed at the restaurant. The model used to detect deviations in equipment performance is analyzed and fault detection thresholds are determined from a statistical basis.

Finally, the results from both laboratory testing and field study are summarized in Section 4. A discussion about the effectiveness of monitoring electrical power consumption to detect improper refrigerant charge, condenser fouling, and evaporator fouling faults is also presented.

The work presented in this paper is similar in some respects to previously published results by other authors (Breuker & Braun 1998; Shen et al. 2009; Kim & Braun 2013; Gouw et al. 2015; Du et al. 2016; Kim & Braun 2016). However, the intent of much of this previous work was focused on understanding how faults can lead to additional energy consumption in direct-expansion equipment and the relationship between performance impacts and fault severity. The goal of the current paper is to examine the potential of using steady-state electrical power measurements to detect different types of faults.

2. SENSITIVITY OF RTU POWER TO FAULTS - LABORATORY TESTING

Laboratory data collected from several RTUs were used to study the impacts different faults have on system performance. The name-plate specifications and description of system components are listed in Table 1 for each system tested. In order to measure the performance impacts of different faults at a range of equipment operating points, psychrometric chambers were used to control the ambient indoor and outdoor conditions. This included operating some of the systems under wet and dry coil conditions. The data analyzed contained the results of injecting common faults into the systems, including improper refrigerant level (both undercharged and overcharged cases), condenser fouling, evaporator fouling.

Table 1. Ratings information for the rooftop units used in this study and descriptions of the components.

System	Rated Capacity	SEER	Refrigerant	Compressor	Expansion Device	Condenser Type
A	5 ton	17.1	R410A	Scroll	TXV	Micro-channel
B[1]	5 ton	-	R410A	Scroll	FXO	Micro-channel
C[2]	5 ton	-	R410A	Scroll	TXV	Finned-tube
D[3]	5 ton	-	R410A	Scroll	FXO	Finned-tube
E (Kim & Braun, 2013)	4 ton	17.5	R410A	Scroll	TXV	Finned-tube
F (Wang *et al.*, 2016)	6 ton	20.5	R410A	Tandem Scroll	TXV (x2)	Finned-tube
G (Shen *et al.*, 2009)	3 ton	12.0	R410A	Scroll	FXO	Finned-tube
H (Shen *et al.*, 2009)	5 ton	10.0	R407C	Scroll	FXO	Finned-tube

[1] System B is a modification to System A where the original expansion device (TXV) was replaced by a short-tube orifice (FXO).

[2] System C is a modification to System A where the original condenser coil (microchannel) was replaced by a finned-tube condenser coil.

[3] System D is a modification to System A where the original expansion valve was replaced with a short-tube orifice (FXO) and the original microchannel condenser was replaced by a finned-tube condenser coil.

The testing included refrigerant charge levels ranging from significantly undercharged to significantly overcharged systems. To characterize the deviation in amount charge contained in the system as compared to a normally charged system, the refrigerant charge level, x_{charge}, was calculated for each test case as

$$x_{charge} = \frac{m_{ref,actual}}{m_{ref,normal}} \times 100\% \quad (1)$$

where $m_{ref,actual}$ is the actual mass of refrigerant in the system and $m_{ref,normal}$ is the amount of mass contained in the system when the system is properly charged (according to manufacturers' specifications). In order to ensure reproducibility between test cases, the systems were placed under vacuum before measuring in refrigerant using a weighing scale. It should also be noted that precaution was taken to reduce the introduction of non-condensable gases by purging the hoses and manifold before adding refrigerant.

Condenser fouling was simulated in two ways: by physically blocking portions of the condenser coil or by reducing the speed of the outdoor fan. While neither method simulates condenser fouling perfectly, the effect of both methodologies causes a reduction in the heat transfer effectiveness and airflow rate. To characterize the extent of condenser fouling imposed, the percent deviation in condenser airflow rate was calculated,

$$x_{ca} = \frac{\dot{V}_{ca,normal} - \dot{V}_{ca,actual}}{\dot{V}_{ca,normal}} \times 100\% \quad (2)$$

where $\dot{V}_{ca,normal}$ is the normal condenser airflow rate when no fouling is imposed and $\dot{V}_{ca,actual}$ is the actual airflow rate measured. Direct measurement of the condenser airflow rate was not possible in any of the experimental setups, so $\dot{V}_{ca,actual}$ was estimated using an energy balance on the condenser coil,

$$\dot{V}_{ca,actual} = \frac{\dot{m}_{ref}(h_{dis} - h_{cro})}{T_{cao} - T_{cai}} \frac{v_{ca}}{c_{p,ca}} \quad (3)$$

where $\dot{m}_{ref}$ is the refrigerant mass flow rate measured using a Coriolis mass flow meter installed on the liquid-line, h_{dis} is the refrigerant enthalpy at the compressor discharge, h_{cro} is the refrigerant enthalpy at the condenser outlet (liquid-line), T_{cao} is the temperature of the air exiting the condenser, T_{cai} is the temperature of the air entering the condenser, v_{ca} is the specific volume of air entering the condenser, and $c_{p,ca}$ is the specific heat of condenser air at constant pressure. When refrigerant leaving the condenser coil is not subcooled, calculating h_{cro} for Equation (3) becomes impossible using only pressure and temperature measurements. Additionally, measuring the mass flow rate of refrigerant becomes unreliable due to the two-phase mixture pass through the Coriolis flow meter. To overcome these limitations, it was assumed that the same fouling level (x_{ca}) results in the same air flow ($\dot{V}_{ca,actual}$) so that test conditions that had subcooled condenser exit states could be used to estimate the actual flow rate.

Similar to condenser fouling, evaporator fouling was simulated in two ways: by physically blocking portions of the evaporator coil or by reducing the indoor blower motor torque. This resulted in lower evaporator air flow rates through the evaporator (but potentially higher air velocities in the case of physically blocked coils). To characterize the extent of evaporator fouling, the percent deviation from normal airflow rate, $\dot{V}_{ea,normal}$, was calculated

$$x_{ea} = \frac{\dot{V}_{ea,normal} - \dot{V}_{ea,actual}}{\dot{V}_{ea,normal}} \times 100\% \quad (4)$$

where $\dot{V}_{ea,actual}$ is the actual airflow rate. In some cases, the volumetric air flow rate through the evaporator was measured directly downstream of the system using calibrated nozzles (ASHRAE 1992). In systems where the airflow was not measured directly, an energy balance was used to estimate the evaporator airflow rate,

$$\dot{V}_{ea,actual} = \frac{\dot{m}_{ref}(h_{suc} - h_{eri})}{h_{eai} - h_{eao}} v_{ea} \quad (5)$$

where h_{suc} is the refrigerant enthalpy at the compressor suction, h_{eri} is the refrigerant enthalpy at the evaporator inlet (assuming an isenthalpic expansion process), h_{eai} is the enthalpy of the air entering the evaporator, h_{eao} is the enthalpy of the air leaving the evaporator, and v_{ea} is the specific volume of evaporator air.

In order to calculate the impact of different faults on electrical power consumption, the percent difference in electrical power caused by a fault, the power impact ratio, r_{power}, was calculated for each test case

$$r_{power} = \frac{\dot{W}_{actual} - \dot{W}_{normal}}{\dot{W}_{normal}} \times 100\% \quad (7)$$

where $\dot{W}_{actual}$ is the actual power of the system and $\dot{W}_{normal}$ is the normal power of the system without faults at the same operating conditions.

2.1 Improper Refrigerant Charge Level Impacts

The impact of refrigerant charge level on steady-state system power consumption is shown in Figure 1 for the Systems A, B, C, and D at several operating conditions. Noticeable differences in instantaneous power impacts can be observed by comparing systems with TXVs and FXOs. Systems with FXO expansion devices tended to have larger impacts on power when significantly undercharged as compared with systems with TXVs having the same type of condenser coils. Moreover, the observed impacts on system power for systems with TXVs were less than 5% at the extreme

undercharged condition for all ambient conditions tested. For systems with FXOs installed, refrigerant charge faults tended to impact system power consumption less during dry coil operation.

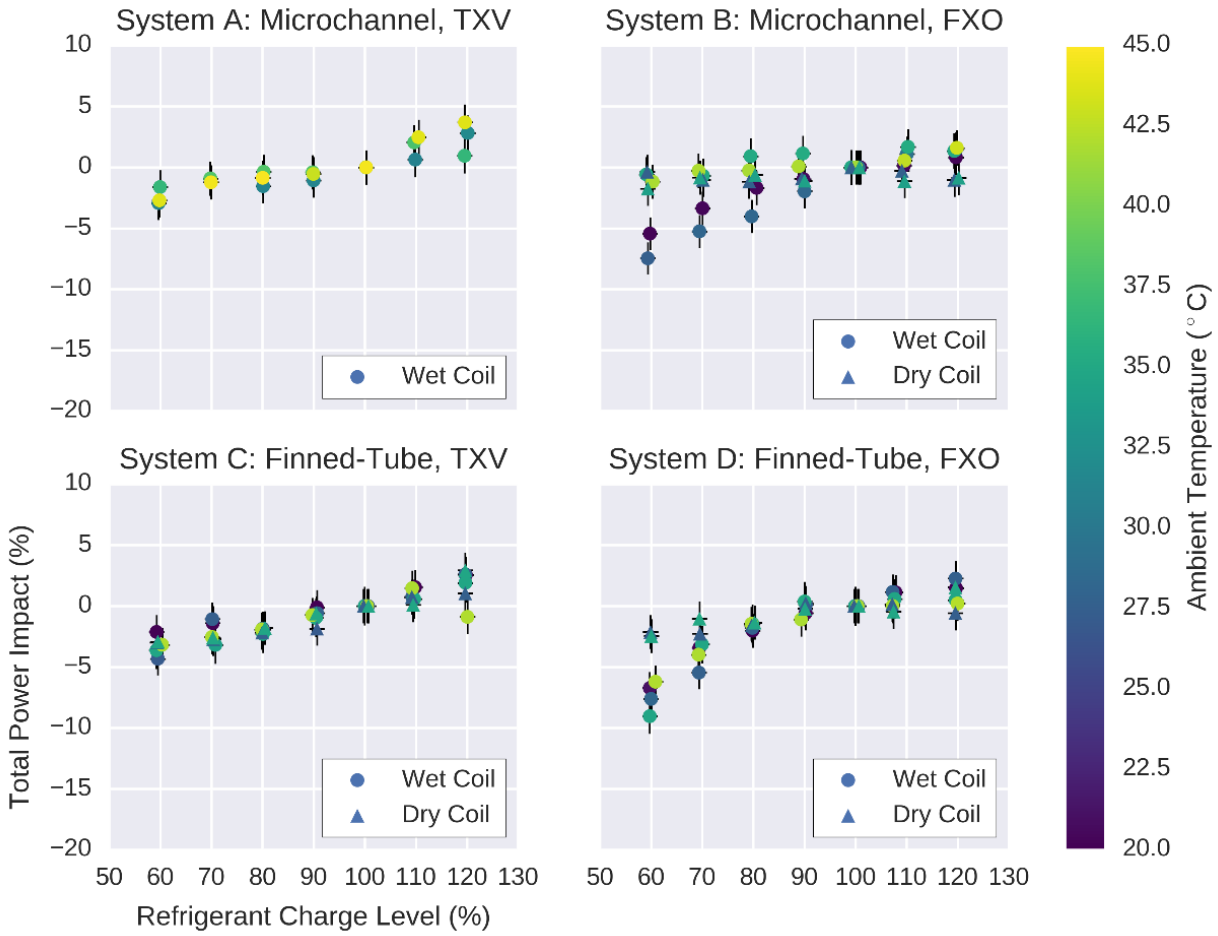

Figure 1. Impacts on instantaneous system power consumption by refrigerant charge faults over a range of steady-state operating conditions observed for Systems A, B, C, and D.

Similar results are shown for Systems E, G, and H in Figure 2. In these tests, Systems E and G were impacted by less than 10% at the most sever undercharged and overcharged conditions tested. Out of all the systems tested, System H had the greatest sensitivity to refrigerant charge level with respect to steady state power consumption. In this system, operating at 60% of the normal charge level resulted in approximately 15% decrease in power consumption. Apart from the working fluid of the system, R407C, the components used in System H are similar to the other systems. Choi and Kim (2004) found similar results and concluded the expansion process of systems using R407C may contribute to significant impacts on performance caused by improper charge levels.

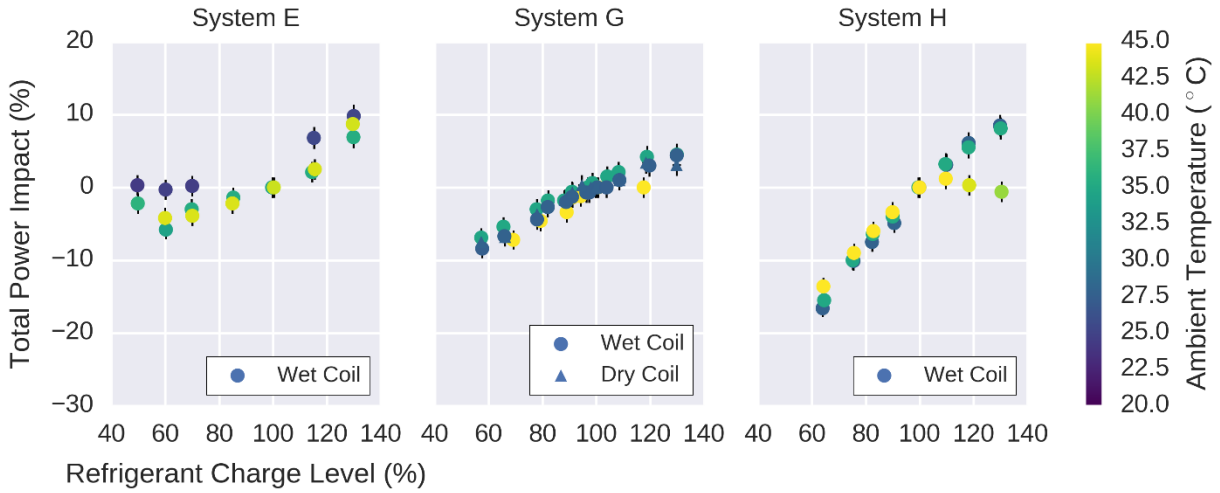

Figure 2. Impacts on instantaneous system power consumption by refrigerant charge faults over a range of steady-state operating conditions observed for Systems E, G and H.

With the exception of one system, the measured steady state system power impacts caused by refrigerant charge faults were less than 10% for all charge levels and ambient conditions tested. This indicates that fault detection algorithms relying on measurements of steady state power must be relatively sensitive in order to reliably detect charge faults. The relatively small impact of refrigerant charge on power occurs because an increased specific work across the compressor is counteracted by a reduced mass flow rate of refrigerant. As a result, refrigerant charge has a more significant effect on cooling capacity and COP than power consumption.

2.2 Condenser Fouling Fault Impacts

The impacts of condenser fouling on the steady state power consumption of Systems E, F, and G are shown in Figure 3 over a range of ambient conditions. The power consumption of the system tends to be positively correlated with the percent reduction in condenser airflow. This is expected since reduction in condenser airflow leads to higher condenser pressures and larger pressure ratios. Thus, compressor power consumption is increased when condenser fouling is present.

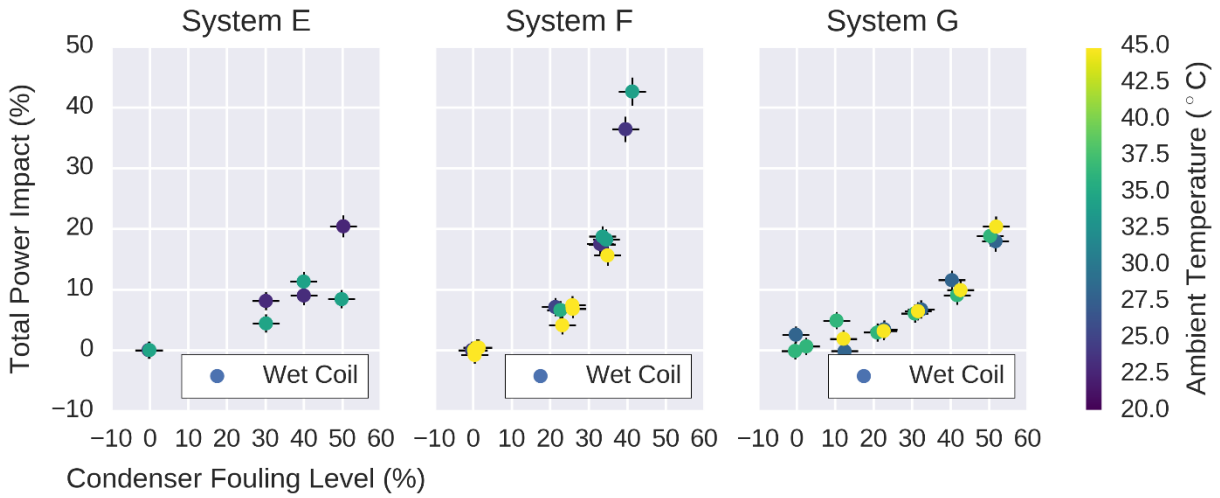

Figure 3. Impacts on instantaneous system power consumption by condenser fouling faults over a range of steady-state operating conditions observed for Systems E, F and G.

Some variation in the magnitude of the impacts on system power consumption exists, as seen in Figure 3. These deviations may be the result of how the condenser fouling was imposed: physically blocking the coil vs. reducing the

outdoor fan speed. Portions of the condenser coil were physically blocked in Systems E and G whereas the fan speed was reduced in System F. The systems with physical blockage may have less impacts due to higher air velocities thru the open portions of the coil, enhancing the heat transfer. In any case, the impacts have similar trends and result in steady-state power impacts greater than 10% for the high fouling levels.

2.3 Evaporator Fouling Fault Impacts

The steady state system power consumption response of Systems E, G, and H to different levels of evaporator fouling are shown in Figure 4. When airflow across the evaporator coil is reduced due to fouling, the coil temperature tends to decrease. This tends to increase latent capacity of the system as well as reduce the low-side and, to a lesser extent, high-side pressures of the system. This tends to decrease the compressor power consumption of the system while also increasing the indoor fan power consumption due to higher coil pressure drop.

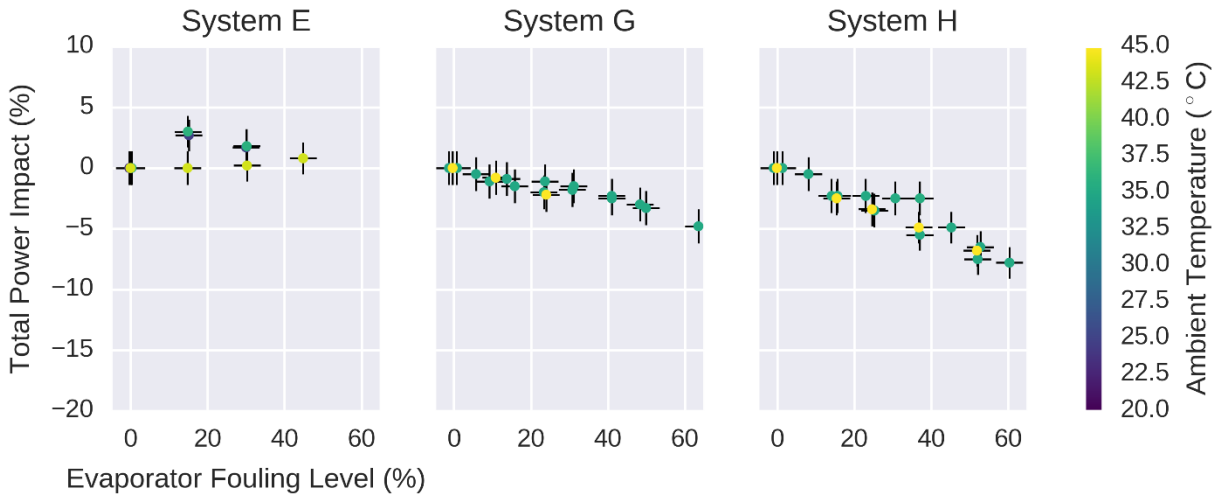

Figure 4. Impacts on instantaneous system power consumption by evaporator fouling faults over a range of steady-state operating conditions observed for Systems E, G and H.

What results is that evaporator fouling impacts steady-state consumption to a lesser extent than condenser fouling. For all the systems shown in Figure 4, less than 10% reduction in steady state power consumption was observed even at relatively large reductions in evaporator airflow rate. This indicates potential difficulty in identifying evaporator fouling faults by monitoring only steady-state power consumption of RTUs.

3. RTU FAULT DETECTION THRESHOLDS USING POWER – FIELD TESTING

Taasevigen et al. (2015) present a fault detection methodology for RTUs capable of detecting operational and degradation faults using only measurements of steady state electrical power consumption and outdoor air temperature. In the methodology, average electrical power consumption of the RTU ($\dot{W}_{ave}$) is modeled using a linear relationship with outdoor air temperature, shown in Equation (8),

$$\dot{W}_{ave} = a_0 + a_1 OAT_{max} \quad (8)$$

where a_0 and a_1 are empirical coefficients that are tuned using operational data collected from the installed RTU. In order to tune the empirical coefficients of Equation (8), data is collected from the unit and automated filtering algorithms are applied. These algorithms include a steady-state filter to remove data during transient operation and clustering algorithms for systems with multiple discrete stages of cooling operation. Furthermore, the empirical parameters are not tuned point-wise. Instead, the power consumed during a sampling interval (e.g. 15-min) and the maximum outdoor air temperature are recorded and are used to train the model.

Once the power consumption of the RTU is modeled using outdoor air temperature as an input, this model is applied to the data over time and compared with actual measurements from the system. As faults develop over time, it is believed that deviations between the measured and the modeled power consumption as functions of outdoor air

temperature will develop. When these deviations become significant enough, indicating the performance of the unit has been impacted by faults, a fault is detected and inspection of the system is recommended.

The methodology proposed by Taasevigen et al. (2015) has many potential benefits due to its limited instrumentation and modeling requirements. Only two sensors are required to implement the fault detection algorithm: a watt meter for system power consumption and a temperature sensor for outdoor air. Furthermore, the outdoor air temperature sensor required could be potentially relaxed if local weather station data is available. An additional advantage of the proposed method is that the model used for fault detection depends only on data collected from the field – no detailed system modeling or psychrometric chamber testing is required. Because of this, the methodology could be applied to newly manufactured units as well as retrofits for systems that are already installed with minimal effort.

The model used in Equation (8) assumes that the power consumption of an RTU can be estimated using only outdoor air temperature. Other factors including return-air condition and sensible and latent loads, are neglected in the model and in practice will contribute to un-modeled noise. The extent of this noise is important since determining statistically acceptable fault detection thresholds depends largely on how well normal performance can be estimated. More noise results in less sensitive fault detection thresholds since it is widely accepted that false alarms cannot be tolerated (Katipamula & Brambley 2005a,b, Yuill & Braun 2013).

In order to assess the effectiveness of using the model shown in Equation (8), the FD (fault detection) methodology proposed by Taasevigen et al. (2015) was applied to several RTUs installed at a small restaurant in Glen Mills, PA. The configurations of five RTUs used in the study are shown in Table 2. A power transducer was installed on each RTU, along with T-type thermocouple temperature sensors for monitoring refrigerant and air side temperature measurements, including outdoor air temperature for the FD methodology. The data acquisition system sampled temperatures, relative humidity, power consumption, and system statuses every minute remote data access was available with a short time lag. The operation of the RTUs was monitored continuously for over two years with minimal interruptions. Data from the summer of 2015 was used in the analysis that follows.

Table 2. Component descriptions of RTUs installed and analyzed at a small restaurant in Glen Mills, PA. A 6th RTU was also monitored, however technical problems with the installed instrumentation made data unreliable for analysis.

System	Stages	Rated Capacity	Refrigerant	SEER	Compressor	Expansion Device	Condenser Type
RTU1	2	15 ton	R410A	17.1	Scroll (x2)	TXV	Micro-channel
RTU2	1	5 ton	R410A	13.0	Scroll	FXO	Finned-tube
RTU3	1	4 ton	R22	10.0	Reciprocating	FXO	Finned-tube
RTU4	1	3 ton	R410A	13.0	Scroll	FXO	Finned-tube
RTU5	1	5 ton	R410A	13.0	Scroll	FXO	Finned-tube

To apply the FD methodology, the average system power consumption and maximum outdoor air temperature over a sampling interval was determined. The average power over an interval was calculated using Equation (9),

$$\dot{W}_{ave} = \frac{\sum_{i=1}^{n} W_{elec,i}}{\sum_{i=1}^{n} \Delta t_{run,i}} \tag{9}$$

where $W_{elec,i}$ is the one-minute energy consumption, $\Delta t_{run,i}$ is the run-time of the system determined using a current transducer monitoring the thermostat call for cooling signal, and n is the length of the sampling interval. In this study, the sampling intervals used were 15-, 30-, and 60-min long (meaning 15, 30, and 60 samples were used to calculate $\dot{W}_{ave}$). Over the same interval, the maximum outdoor air temperature was determined as well,

$$OAT_{max} = \max\{ OAT_i \} \quad \text{for } i = 1, \ldots, n. \tag{10}$$

The data was further filtered by eliminating points where less than 70% of the sampling interval used mechanical cooling (compressor was on).

Using measured data collected from the RTUs installed, the average power consumption of each unit was modeled using Equation (8). The data collected from RTU1 for both stages of cooling operation, as well as the model estimates are plotted in Figure 5. In comparison to the linear models in Figure 5, the measured data show approximately linear behavior with respect to outdoor air temperature. The return air temperature measured at RTU1 has also been mapped in Figure 5, however the data show minimal impact of return air temperature on power consumption or residuals. The

root-mean-square error (RMSE) of the models generated for the 1st and 2nd stage operation of RTU1 are 2.52% and 3.90% respectively.

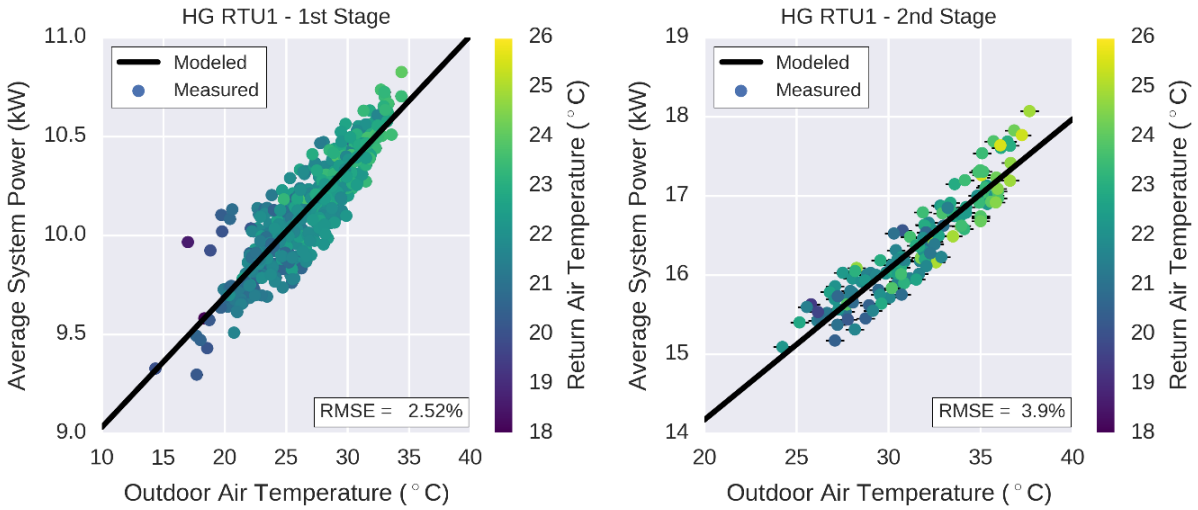

Figure 5. Measured RTU1 system power consumption for both stages of cooling operation as a function of measured outdoor ambient temperature. The data is modeled by fitting Equation (8) to the measured data.

Similarly, the measured system power of RTU2 and RTU3 are shown as functions of the outdoor air temperature in Figure 6. In comparison to the model performance of RTU1, the model approximates the measured power consumptions more or less equally well. The RMSE of the RTU2 and RTU3 models are 3.27% and 4.96% respectively. The results show that the model shown in Equation (8) is able to capture the general trend in power consumption observed in the actual building with some expected uncertainty.

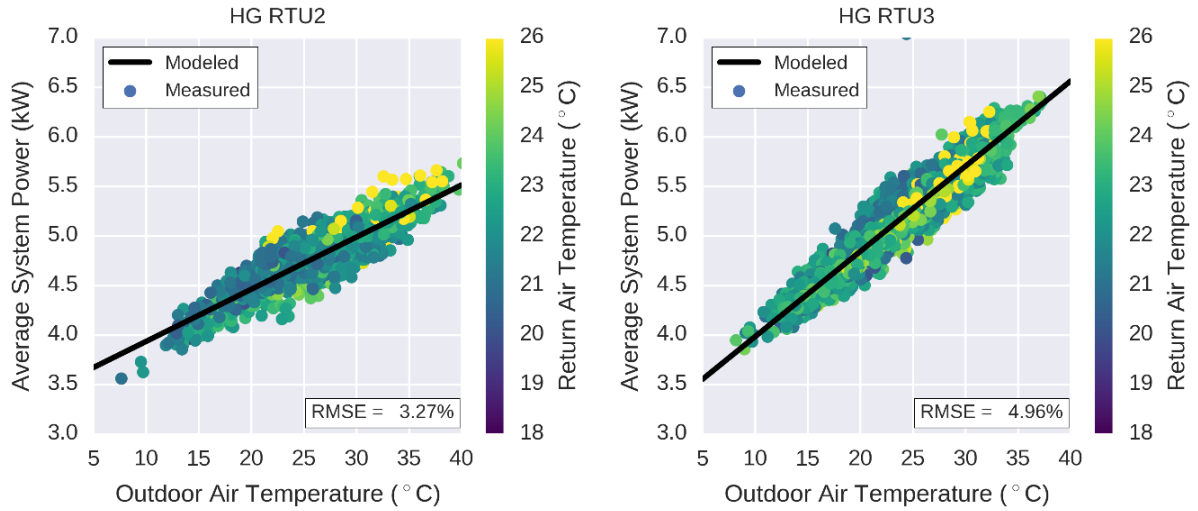

Figure 6. Measured RTU1 system power consumption for both stages of cooling operation as a function of measured outdoor ambient temperature. The data is modeled by fitting Equation (8) to the measured data.

A comparison of the RMSE obtained by fitting Equation (8) to the measured data is shown in Table 3 for each RTU and different sampling intervals for filtering. It was observed that larger sampling intervals resulted in smaller RMSE which may indicate using a longer sampling interval reduces the impacts of un-modeled variables affecting system power consumption like differences in return-air temperature and humidity and the building cooling load. RTU4 and RTU5 tended to have larger RMSE errors than the other RTUs monitored. These RTUs were used to condition the entry way of the restaurant and the kitchen respectively. The kitchen area would have large variations in internal gains

that cannot be captured with ambient temperature dependence, whereas the entry way could have significant time-varying coupling to the ambient due to door openings that depend upon restaurant traffic.

Table 3. Root-mean-square errors (RMSE) of ambient temperature based system power model for RTUs installed at restaurant field test site using different length filtering lengths. Using RMSE of 60-min window, the minimal impact on power that is can be detected at 95.0%, 99.0%, 99.9% statistical confidence is calculated.

	RMSE			60-min Impact Thresholds		
System	15-min Window	30-min Window	60-min Window	95.0% CI	99.0% CI	99.9% CI
RTU1, 1st Stage	3.1%	2.7%	2.5%	±4.1%	±5.8%	±7.7%
RTU1, 2nd Stage	4.3%	4.0%	3.9%	±6.4%	±9.1%	±11.2%
RTU2	4.7%	3.6%	3.2%	±5.3%	±7.4%	±9.9%
RTU3	5.7%	4.0%	4.9%	±8.1%	±11.4%	±15.1%
RTU4	9.7%	9.0%	8.8%	±14.5%	±20.5%	±27.2%
RTU5	10.4%	8.6%	8.0%	±13.1%	±18.6%	±24.7%

The data observed at the restaurant were used to determine fault detection thresholds based on the measured model residuals. A probabilistic approach originally proposed by Rossi and Braun (1997) was used where the expected classification error is used to define fault detection thresholds. Figure 7 shows pictorially how distributions for the measured power and modeled power can be sampled and the area of overlap, corresponding to the classification error, can be calculated.

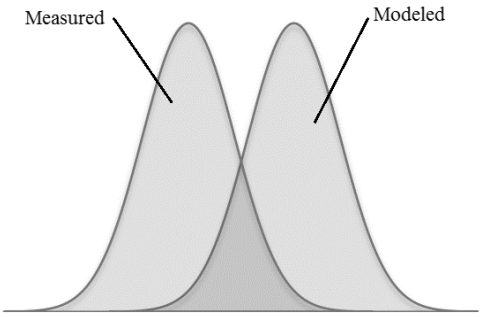

Figure 7. The probability that the measured power has deviated from the modeled power can be estimated by integrating the area of overlap between the two sample distributions. Faults can be detected by setting a threshold for the minimum area of overlap that corresponds to normal behavior.

If it is assumed that the predicted power and the measured power have the same standard deviation (stemming from the un-modeled factors previously described), the classification error can be calculated for normally distributed points using Equation (11),

$$p_{error} = \left[1 + \text{erf}\left(\frac{\mu_{meas} - \mu_{model}}{\sigma}\right)\right] \tag{11}$$

where the $\theta = \mu_{meas} - \mu_{model}$ is the difference between the sample means of the measured and model steady state power consumption, σ is the standard deviation of the distributions, and erf is the error function. Using the standard deviation of the model residuals for each RTU, the percentage difference in predicted power consumption of the model and measured data required for the classification error to be 5%, 1%, and 0.1% were calculated. These results of these calculations for the 60-min sampling interval results are shown in Table 3 for each system. These thresholds correspond to minimum deviation required for there to be less than 5%, 1%, or 0.1% chance of a false alarm and missed detection.

4. DISCUSSION AND CONCLUSIONS

An analysis of the statistical fault detection thresholds show that more conservative thresholds result in greater required deviations between the models representing normal performance and measured observations. In order to minimize false alarms, larger fault detection thresholds must be used. However, this results in less sensitive fault

detection sensitivity. Comparing the fault detection thresholds calculated from field data with the measured impacts on steady state power consumption of the RTUs tested in the laboratories shows that using only measurements of power consumption and outdoor air temperature may be problematic. In order to detect different types of faults commonly affecting RTUs, a fault detection algorithm must be relatively sensitive since some important faults (e.g., refrigerant charge) do not have a large impact on power consumption even for severe faults. Based on the data collected from the field, sensor and un-model noise causes relatively high uncertainty in comparison to the fault impacts.

More specifically, RTUs 2-5 at the field site required deviations in power consumption greater than 10% in order to guarantee false alarm rates less than 0.1%. This indicates that only condenser fouling faults may be detected with any regularity. The refrigerant charge faults and evaporator fouling faults resulted in less than 10% deviations in steady-state power consumption and thus would not be identified using the applied fault detection criteria. Furthermore, the fault impacts considered in the laboratory setting only included scenarios with one fault affecting the systems at a time. During normal operation of systems, multiple faults may develop simultaneously. It may be possible that faults with different trends on equipment energy consumption may reduce overall power impacts when occurring simultaneously.

Several common faults were not considered in this work, including compressor valve leakage, liquid-line restrictions, and the presence of non-condensable gases in the refrigerant circuit. The presence of non-condensable gases tends to increase high-side pressure like condenser fouling faults which could indicate monitoring steady state power as a function of outdoor air temperature could be used to detect this type of fault. Several authors have published laboratory test results showing impacts of power consumption of compressor valve leakage faults and liquid-line restrictions are relatively minor (Breuker & Braun 1998; Shen et al. 2009; Kim & Braun 2013; Gouw et al. 2015; Du et al. 2016; Kim & Braun 2016). Wang et al. (2016) present the results of injecting different faults on several RTUs installed at two convenience stores in Florida. The results showed evaporator fouling faults and compressor valve leakage faults had minimal impacts on steady-state power consumption while high levels of condenser fouling significantly impacted power consumption (Wang et al. 2016).

Possible improvements to the methodology described by Taasevigen et al. (2015) may improve the performance of the fault detection methodology. For instance, including measurements of the return air temperature and humidity may eliminate some of the noise which would decrease the fault detection thresholds. Other possibilities include monitoring cooling capacity or COP over time in order to identify faults that result in large impacts on these performance indicators. Laboratory and field study results of the impacts on capacity and COP for RTUs have been presented by Hjortland and Braun (2016) and Wang et al. (2016) respectively. While these solutions would result in higher instrumentation and component costs, it may result in greater energy and cost saving potential by detecting faults earlier with less false alarms.

REFERENCES

Armstrong, P.R., Laughman, C.R., Leeb, S.B., and Norford, L.K. (2006). Detection of Rooftop Cooling Unit Faults Based on Electrical Measurements. *HVAC&R Research* 12(1): 151–176.

ASHRAE. (1992). *Standard Method for Laboratory Airflow Measurements*. ANSI/ASHRAE Standard 41.2-1987 (RA93). American Society of Heating, Refrigeration, and Air-Conditioning Engineers. Atlanta, GA.

Breuker, M. and Braun, J. (1998). Common Faults and Their Impacts for Rooftop Air Conditioners. *HVAC&R Research*, 4(3): 303–318.

Choi, M. and Kim, Y. (2004). Influence of the expansion device on the performance of a heat pump using R407C under a range of charging conditions. *International Journal of Refrigeration*, 27(4): 378–385.

Du, Z, Domanski, P.A. and Payne, W.V. (2016). Effect of common faults on the performance of different types of vapor compression systems. Applied Thermal Engineering, 98: 61–72.

Gouw, S., Faramarzi, R., and Ahmed, J. (2015), Evaluating the Effects of Common Faults on a Commercial Packaged Rooftop Unit, ET13SCE7050, Southern California Edison, Rosemead, CA.

Hjortland, A. L. and Braun, J. E. (2016). Development of an Embedded RTU FDD System using Open-Source Monitoring and Control Platform. International Refrigeration and Air Conditioning Conference. West Lafayette, IN.

Katipamula, S. and Brambley, M.R. (2005) Methods for Fault Detection, Diagnostics, and Prognostics for Building Systems—A Review, Part I, *HVAC&R Research*, 11(1): 3-25.

Katipamula, S. and Brambley, M.R. (2005) Methods for Fault Detection, Diagnostics, and Prognostics for Building Systems—A Review, Part II, *HVAC&R Research*, 11(2): 169–187.

Kim, W. and Braun. J.E. (2013). Performance Evaluation of a Virtual Refrigerant Charge Sensor, International Journal of Refrigeration, 36(3): p. 1130–1141.

Kim W. & Braun, J. E. (2016) Development and evaluation of virtual refrigerant mass flow sensors for fault detection and diagnostics. *International Journal of Refrigeration*, 63(2): 184–198.

Li, H. and Braun, J.E. (2007). A Methodology for Diagnosing Multiple Simultaneous Faults in Vapor-Compression Air Conditioners, *HVAC&R Research*, 13(2): 369–396.

Rossi, T.M. and Braun J.E. (1997). A Statistical, Rule-Based Fault Detection and Diagnostic Method for Vapor Compression Air Conditioners, *HVAC&R Research*, 3(1): 19–37.

Shen, B, J.E. Braun, and E.A. Groll. (2009). Improved methodologies for simulating unitary air conditioners at off-design conditions. International Journal of Refrigeration 32(7): 1837–1849.

Taasevigen, D.J., Brambley, M.R., Huang, Y., Lutes R.G., and Gilbride, S.P. (2015). Field Testing and Demonstration of the Smart Monitoring and Diagnostic System (SMDS) for Packaged Air-Conditioners and Heat Pumps, PNNL-24000, Pacific Northwest National Laboratory, Richland, WA.

Wang, J., Gorbounov, M., Yasar, M., Reeve, H., Hjortland A.L., and Braun J.E. (2016). Lab and Field Evaluation of Fault Detection and Diagnostics for Advanced Roof Top Units. *International Refrigeration and Air Conditioning Conference*. West Lafayette, IN.

Yuill, D.P. and Braun, J.E. (2013). Evaluating the performance of fault detection and diagnostics protocols applied to air-cooled unitary air-conditioning equipment, *HVAC&R Research*, 19(7): 882–89.

ACKNOWLEDGEMENT

This work is funded by Consortium for Building Energy Innovation (formally known as Energy Efficient Buildings Hub), sponsored by the Department of Energy under Award Number DE-EE0004261.

DISCLAIMER

the United States Government or any agency thereof. The views and opinions of authors expressed herein do not necessarily state or reflect those of the United States Government or any agency thereof.